Available online at www.sciencedirect.com
SCIENCE DIRECT®
International Journal of Heat and Mass Transfer 49 (2006) 2864–2876
International Journal of HEAT and MASS TRANSFER
www.elsevier.com/locate/ijhmt

# Improved analytical solution for inverse heat conduction problems on thermally thick and semi-infinite solids

P.L. Woodfield [a,1], M. Monde [b,*], Y. Mitsutake [b,2]

[a] Institute of Ocean Energy, Saga University, 1 Honjo-machi, Saga 840-8502, Japan
[b] Department of Mechanical Engineering, Saga University, 1 Honjo-machi, Saga 840-8502, Japan

Received 7 October 2005
Available online 17 April 2006

**Abstract**

Analytical solutions to inverse heat conduction problems with a far-field boundary condition are derived for one- and two-dimensional problems using a Laplace transform technique. Accuracy of the predictions is improved by superposition of successive corrections to the function used to approximate the measured data. Long-term history of high frequency modes in both time and space is neglected noting that these components do not penetrate deeply into the solid. The two-dimensional solution is a relatively simple extension of the one-dimensional formulation. The present results are most useful for determining surface temperature and heat flux based on measured data from a row of sensors at a single depth below the surface and a known or measured boundary condition far from the surface.


*Keywords:* IHCP; Analytical solution; Semi-infinite solid

## 1. Introduction

The focus of this present article is thermally thick and semi-infinite solids. As is well known, the Fourier number, $at/z^2$ is a key dimensionless parameter for relating time and length scales for heat conduction in solids. For example, if $at/H^2 < 0.1$, where $H$ is the thickness of a one-dimensional plate then for practical purposes, the plate may be treated as a semi-infinite solid (to better than 1% accuracy) since the conditions at the surface have a very small effect at the position $z = H$ for these short time scales.

Consider also the unsteady one-dimensional inverse heat conduction problem (IHCP) where the surface temperature is unknown. Heat conduction is governed by a second-order partial differential equation requiring for closure an initial condition and two spatial boundary conditions (at $z = z_1$ and $z = z_2$). All inverse solutions will have trouble resolving time scales corresponding to $at/z_1^2 < 0.1$, where $z_1$ is the depth of the closest sensor to the surface. This is simply because the first sensor hardly detects surface temperature fluctuations with such a small time period. Therefore for good time resolution, the first sensor should be placed close to the surface. The story is different for the second boundary at $z = z_2$, however. The effect of its location on inverse solutions is the key interest in this study.

In principle the location of the second boundary should not be critical for closing the mathematical problem. Moreover, the nature of the boundary at $z_2$ whether it is measured temperatures or known heat flux or even the case of the semi-infinite solid ($z_2 \to \infty$) should not greatly influence the result. However in practice as $z_2$ becomes larger (i.e., $at/z_2^2$ becomes smaller) the solid bounded by $0 < z < z_2$ tends to 'remember' more long-term thermal history. Therefore for analytical methods, additional effort is required to ensure approximating functions and inverse solutions retain extra details of the thermal history if $z_2$ is large. This makes such problems more challenging than IHCPs for 'thin' solids. Here, and throughout this article,

* Corresponding author. Tel.: +81 952 28 8608; fax: +81 952 28 8587.
*E-mail addresses:* peter@me.saga-u.ac.jp (P.L. Woodfield), monde@me.saga-u.ac.jp (M. Monde), mitutake@me.saga-u.ac.jp (Y. Mitsutake).
[1] Tel.: +81 952 26 3870; fax: +81 952 28 8595.
[2] Tel.: +81 952 28 8616; fax: +81 952 28 8587.

0017-9310/$ - see front matter © 2006 Elsevier Ltd. All rights reserved.
doi:10.1016/j.ijheatmasstransfer.2006.01.050

**Nomenclature**

| | |
|---|---|
| $a$ | thermal diffusivity |
| $A$ | arbitrary constant coefficient in Eq. (A5a) representing magnitude of oscillation |
| $B$ | any length appearing in the exponentials of the solution in Laplace space |
| $C_1$ | factor for reducing size of consecutive data windows (Eq. (7)) |
| $C_2$ | Fourier number to decide how much future data to include (Eq. (8)) |
| $C_3$ | Fourier number to decide size of first window in 2D calculation (Eq. (20)) |
| $F_j$ | time function to approximate the size of the coefficient for the $j$th eigenfunction |
| $g_n$ | function associated with solution for known heat flux boundary |
| $G_{i,k}$ | coefficient for inverse solution |
| $h$ | function defined by Eq. (A10) |
| $H$ | thickness of finite solid in $z$-direction |
| $L$ | length of two-dimensional solid in $x$-direction |
| $L\{\}$ | Laplace transform operator |
| $m_j$ | $j$th eigenvalue |
| $N_j$ | number of eigenfunctions minus one |
| $N_k$ | order of approximating polynomial |
| $N_{\min}$ | minimum number of data points permitted for smallest window |
| $N_{\text{corr}}$ | number of corrections applied to the polynomial fit |
| $P_{i,k}$ | coefficient in approximating polynomial |
| $r$ | radial position |
| $R$ | radius of cylinder |
| $s$ | Laplace transform variable |
| $t$ | time |
| $t*$ | start of data window for two-sensor solution |
| $t_f$ | finish of data window for one-sensor solution |
| $t_i$ | start of data window for $i$th correction to approximating function |
| $T$ | temperature |
| $T_{\text{surf}}$ | surface temperature |
| $T_{\text{meas}}$ | measured temperature data |
| $T_{\text{corr}}$ | temperature difference between approximating function and measured data |
| $x$ | distance along the surface in two-dimensional problem |
| $z$ | depth from surface |
| $z_1$ | depth of sensor 1 |
| $z_2$ | depth of sensor 2 |

*Greek symbols*

| | |
|---|---|
| $\Gamma()$ | gamma function |
| $\zeta$ | dimensionless length defined by Eq. (A7a) |
| $\theta$ | surface temperature correction |
| $\lambda$ | thermal conductivity |
| $\tau$ | dimensionless time defined by Eq. (A7c) |
| $\phi$ | function appearing in Eq. (A6a) |

the expression 'thermally thick' is understood to mean that for the time scale of interest, the Fourier number based on the thickness of the solid (or position of $z_2$) is small (say less than one). In a similar manner, the expression 'long-term history' refers to temperature data such that the Fourier number based on the depth of the deepest sensor and the time back to this data is significantly greater than unity.

Although limited to fairly simple geometry, explicit analytical solutions to IHCPs are very fast computationally and are of fundamental importance to understanding all IHCPs. Burggraf [1], Sparrow et al. [2], Imber [3] and Shoji [4] have among others made important contributions to the analytical approaches for solving IHCPs. Based on these earlier studies but using polynomials in the half-power of time to approximate the measured data, Monde and co-workers [5–8] were able to derive successful analytical solutions to IHCPs in both one and two dimensions. The most accurate results were obtained for cases where the temperature sensors were located at two different depths, $z_1$ and $z_2$, from the surface of the solid. In particular they recommended that $z_1$ be as close as practical to the surface. The minimum prediction time was found to improve if $z_2$ also was close to the surface [7]. In this way treatment of the IHCP could be reduced to application of the inverse solution to a relatively thin layer from $z = 0$ to $z = z_2$ and difficulties associated with treatment of thick solids were largely avoided.

Starting with Monde's formulation [7,8], Woodfield et al. [5] made use of the fact that the top layer from the surface to $z_2$ need not be overly thick in well-designed experiments [9,10] to justify neglecting the long-term history of the data. They demonstrated that by limiting the range of data used by the inverse solution to a small window, the predictions from the analytical solutions by Monde et al. [6–8] improved for data with complicated fluctuations. The Fourier number for the sensor at the second depth determined the minimum size of the data window. Again their study focused on the cases with sensor readings at two depths in the solid.

In the approach with sensors at two depths, even when applied to a semi-infinite solid, no reference is made to the semi-infinite boundary condition. This makes the method very flexible and same solution is applicable to a range of problems since the far-field boundary condition is not used. However, in cases where the semi-infinite boundary condition is actually valid or some other boundary condition is known then in principle, one row of sensors could become redundant. This is highly desirable since experimental apparatus can become simpler or if the

additional sensors are not removed the extra information could be used to confirm the results or even determine the thermal diffusivity of the material [6]. Monde et al. [6–8] had some success with inverse solutions based on a single depth of sensors although the reported accuracy was not as good as that for two rows of sensors [8]. In the present article we propose a modified procedure that greatly extends the applicable time range for the Laplace transform analytical solution to IHCPs with sensors at a single depth in semi-infinite and thick solids. Moreover, by changing the boundary condition in the formulation, the procedure also can be applied to the case with sensors at two depths but with the added flexibility that the second depth can be far from the surface and fewer sensors are required. The procedure is applied to both one- and two-dimensional problems.

## 2. Formulation of inverse solution

For the purposes of illustrating the present technique consider the one-dimensional case of a single sensor at depth $z_1$ below the surface in a semi-infinite solid. The problem is formulated as in Eq. (1).

$$\frac{\partial T}{\partial t} = a\frac{\partial^2 T}{\partial z^2} \tag{1a}$$

$$T|_{t=t_0} = T_0 \tag{1b}$$

$$T|_{z\to\infty} = T_0 \tag{1c}$$

$$(T-T_0)|_{z=z_1} = \sum_{k=0}^{N_k} P_{0,k}\frac{(t-t_0)^{k/2}}{\Gamma((k/2)+1)} + \sum_{i=1}^{N_{\text{corr}}}\sum_{k=0}^{N_k} P_{i,k}\frac{(t-t_i)^{k/2}}{\Gamma((k/2)+1)} \tag{1d}$$

Suppose we have some experimental data in the range from time, $t_0$, to time, $t_f$, and we wish to know the surface temperature at time, $t$, where $t$ is a little before $t_f$. The goal of Eq. (1d) is to approximate the measured data from time, $t_0$, to $t_f$. In particular, the fit should be very accurate near the time of interest, $t$, and low frequency components from the long-term history should be retained. The first summation on the right of Eq. (1d) involving the coefficients, $P_{0,k}$ is a least-squares approximation to the data from $t=0$ to $t_f$. The second summation involving the coefficients, $P_{i,k}$ is the key contribution of this present study. It represents a set of corrections to the original fit to make Eq. (1d) better approximate the data near time, $t$. For example, the sum from $k=0$ to $N_k$ with coefficients, $P_{1,k}$ is a correction to the data fit in the range from time, $t_1$, to $t_f$. The total number of corrections is denoted as $N_{\text{corr}}$. Note that $P_{i,k}$ is a constant for $t > t_i$ and zero for $t < t_i$.

The ranges for first estimate and corrections in Eq. (1d) are illustrated graphically in Fig. 1(a). The case considered in the figure is computer-generated data for a semi-infinite solid where the exact solution for the boundary heat flux is a square wave in time. Because the size of the data window becomes smaller and each correcting polynomial in Eq. (1d) has the same number of coefficients, the data can be approximated well near time, $t$. As in [5], the present approach requires that the data fit and inverse solution be applied independently for each point in time.

By the principle of superposition it is easy to see that the problem defined by Eqs. (1a)–(1d) is simply the summation of a number of problems of the form given by Eq. (2).

$$\frac{\partial \theta}{\partial t} = a\frac{\partial^2 \theta}{\partial z^2} \tag{2a}$$

$$\theta|_{t=t_i} = 0 \tag{2b}$$

$$\theta|_{z\to\infty} = 0 \tag{2c}$$

$$\theta|_{z=z_1} = \sum_{k=0}^{N_k} P_{i,k}\frac{(t-t_i)^{k/2}}{\Gamma((k/2)+1)} \tag{2d}$$

Eq. (2) is the basic form defining the IHCP tackled by Monde et al. [7] for the one-dimensional semi-infinite solid. The gamma function, $\Gamma()$, is inserted in the denominator of Eqs. (1d) and (2d) to make the Laplace transform a little tidier. After taking Laplace transforms and solving in Laplace space Eq. (3) results.

$$\overline{\theta} = \sum_{k=0}^{N_k} \frac{P_{i,k}}{s^{(k/2)+1}} e^{-\sqrt{s/a}(z-z_1)} \tag{3}$$

Substituting $z=0$, replacing the exponential with a series expansion and returning to the time domain, the solution to Eq. (2) is given by Eq. (4).

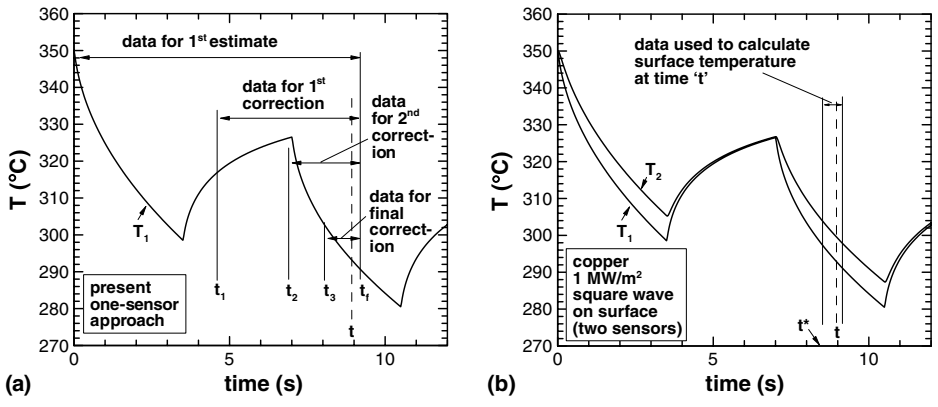


Fig. 1. Data ranges used to calculate surface temperature and heat flux at time '$t$', (a) present one-sensor approach and (b) two-sensor approach [5].

$$\theta = \sum_{k=-1}^{N_k} \frac{G_{i,k}(t-t_i)^{k/2}}{\Gamma((k/2)+1)} \tag{4}$$

where $G_{i,k}$ is the coefficient of $s^{-((k/2)+1)}$ of the series satisfying Eq. (5).

$$\sum_{k=-\infty}^{N_k} \frac{G_{i,k}}{s^{(k/2)+1}} = \sum_{n=0}^{N_k} \frac{P_{i,n}}{s^{(n/2)+1}} \sum_{j=0}^{\infty} \frac{1}{j!}\left(\frac{z_1}{\sqrt{a}}\right)^j s^{j/2} \tag{5}$$

Note that in Eq. (5) we need only consider terms in the range from $k=-1$ to $k=N_k$ and that values for $G_{i,k}$ may be extracted easily in a computer program using a nested loop [5]. Further details of this approach to IHCPs can be found in Ref. [5–8]. Thus by the result in Eq. (4) and the principle of superposition, the final solution to Eqs. (1a)–(1d) for the temperature at the surface is given by Eq. (6). The surface heat flux may be obtained by differentiating Eq. (3) with respect to $z$, multiplying by $-\lambda$ and then proceeding in the same manner as for temperature. Alternatively, the same analytical result for surface heat flux may be obtained by directly differentiating the results given in Appendix 2 with respect to $z$.

$$T|_{z=0} - T_0 = \sum_{i=0}^{N_{\text{corr}}} \sum_{k=-1}^{N_k} \frac{G_{i,k}(t-t_i)^{k/2}}{\Gamma((k/2)+1)} \tag{6}$$

It should be mentioned in passing that Eq. (4) is derived from an approximate inverse Laplace transform since replacing the exponential with the truncated series expansion does not necessarily account for the full effect of the branch point at $s=0$. Nevertheless, we have found by numerical experiment that if Eq. (2d) is accurate then the accuracy of Eq. (4) with $z<z_1$ diminishes only as $a(t-t_i)/z_1^2 \to 0$ in the region where all inverse solutions become questionable.

## 3. Implementation

To implement the proposed solution procedure, it is not necessary to store simultaneously all of the coefficients, $P_{i,k}$, in Eq. (1d). Fig. 2 shows how corrections and updates to the solution may be applied in an iterative manner resulting in the surface temperature at time $t$, as given by Eq. (6).

In Fig. 2, $T_{\text{surf}}$ is the unknown surface temperature and $\{T_{\text{meas}}\}$ is the measured temperature data at depth $z=z_1$. The curly brackets, $\{\}$ are used for a set of discrete points. $\{T_{\text{corr}}\}$ represents the difference between the approximating equation (Eq. (1d)) and the measured data for $i-1$ iterations of the loop in Fig. 2. The basic inverse solution, $\theta_{\text{surf}}$ in Fig. 2 is specified by Eq. (4) once appropriate coefficients have been selected for the polynomial fit to the required correction for loop $i$. For each correction, the size of the data window, $(t_f - t_i)$, reduces by a factor of $C_1$ (where $0<C_1<1$) as in Eq. (7). For the present study $C_1=0.5$ is found to be near the optimum in terms of computational speed and accuracy.

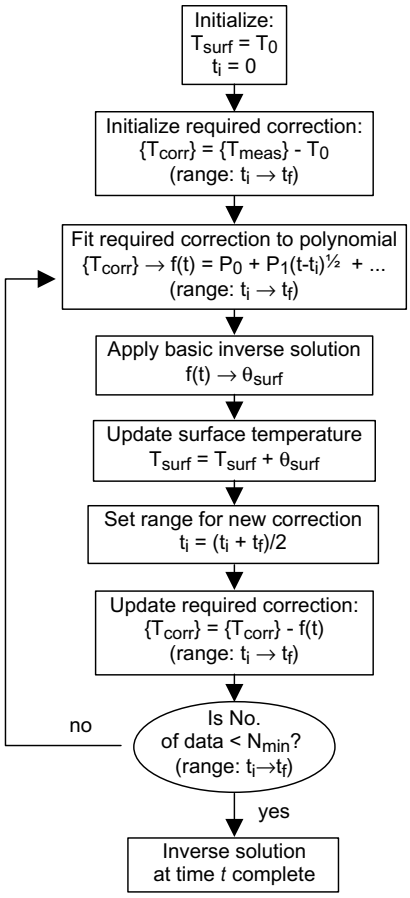


Fig. 2. Algorithm for implementing present inverse solution.

$$t_{i+1} = t_f - C_1(t_f - t_i) \tag{7}$$

The time, $t_f$, in Eq. (7) is chosen such that the Fourier number based on the depth of the thermocouple and the time after $t$ is given by Eq. (8), where $C_2$ is a number of an order less than one (here we have taken $C_2=0.8$).

$$a(t_f - t)/z_1^2 = C_2 \tag{8}$$

Eq. (8) allows more than enough future data to be included in the fit to help account for the delay required for a change on the surface to penetrate to $z_1$. Finally, the loop terminates when the window size becomes so small that the number of data points in the range $(t_f - t_{i+1})$ becomes of a similar order of magnitude as the number of coefficients in the approximating polynomial. In the present study we use $(t_f - t_{i+1}) < N_{\min}$ where $N_{\min}=8$ for the case where $N_k=5$.

## 4. Motivation for proposed form of approximating function

The goal of Eq. (1d) is to approximate the measured data from the sensor. Ideally, it would be desirable to find a single function, which could capture accurately whole range of data and then the surface temperature at every point in time could be evaluated immediately. However, this is not easily done and is in fact one of the key issues for applying analytical inverse solutions to practical data.

As mentioned above, in the present study we content ourselves to apply different data fits and the inverse solution separately for each point in time. This is more computationally expensive than a single equation but allows for a consistently accurate treatment. Moreover, with modern digital computers the computation time for the present analytical solution is not a major concern. For example, on a modest Pentium IV personal computer with a clock speed of 1.8 GHz, a one-dimensional problem with 400 data points using the present procedure requires less than 2 s to evaluate the surface temperature and heat flux at 400 different values of $t$.

To further discuss the merits of Eq. (1d), it is helpful to consider a concrete example. Fig. 3 illustrates how Eq. (1d) approximates the data from time zero to $t_f$. As in Fig. 1, the case given is computer-generated data for a square-wave heat flux on the surface of a semi-infinite solid. The material is copper, and the maximum heat flux, 1 MW/m$^2$, and the depth $z_1 = 2$ mm are of the order of magnitude appearing in the authors' experimental work for quenching of high temperature surfaces [9,10].

The finer solid line in Fig. 3 shows to what degree a least-squares fit of a single polynomial in the half-power of time can approximate the whole range from time zero to $t_f$. This is equivalent to using only the first series involving $P_{0,k}$ in Eq. (1d). It is quite clear that the finer solid line captures the approximate trend of the data but does not accurately fit the data in the important region leading up to the time of interest, '$t$'.

The heavy solid line in Fig. 3 shows the final approximation to the data using Eq. (1d) where five corrections have been employed. In this case the fit is very good close to time, $t$. It should be noticed in Fig. 3 that for time less than about 13 s, the accuracy of the solid line fit to the data deteriorates somewhat and tends to fluctuate around the given data. This is not a major concern since it can be demonstrated that high frequency components do not penetrate deeply into the solid [11]. Thus, high frequency fluctuations in the long-term history are quickly damped and have little effect on the result at time '$t$'. It is important, however, that higher frequency modes in the data close to the time of interest be resolved correctly. This provides the motivation for using successively smaller correcting windows as illustrated in Fig. 1(a) and Eq. (7) close to time '$t$'. On the other hand, low frequency modes do penetrate deeply into the solid so any suitable approximating function should retain low frequency fluctuations a considerable time before the time of interest, '$t$'.

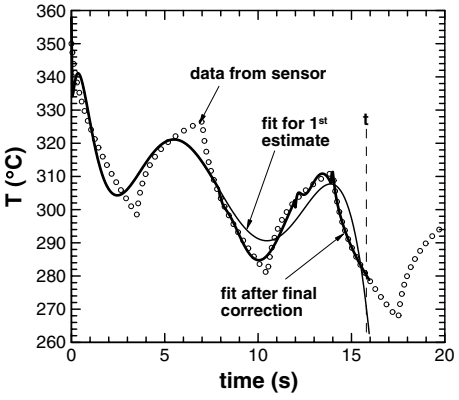


Fig. 3. Fit to data in order to estimate the surface temperature and heat flux at time '$t$'.

It may be worth mentioning here that in the case of sensors at two depths reasonably close to the surface, we need not concern ourselves with the low-frequency modes in history of the data. This is because the sensors at the second depth automatically detect any thermal waves returning from deep within the solid. Thus the single window shown in Fig. 1(b) is justified for the case of sensors at two depths but some of the long-term history must be retained for the single-sensor case in Fig. 1(a).

## 5. Extension to problems involving thick finite solids

The present method is not limited to problems involving semi-infinite solids. In principle, any fundamental solution to a heat conduction problem with a zero initial condition and one homogeneous boundary condition (or three for 2D) could be applied in place of $\theta_{\text{surf}}$ in Fig. 2. However for the present kind of problems, success is more likely if the analytical solution also has been designed specifically with thermally thick solids in mind. Consider the important case of a one-dimensional slab of finite thickness, $H$, where the heat flux is zero at $z = H$. The formulation of the basic problem is the same as Eq. (2) except that Eq. (2c) is replaced by Eq. (9).

$$\left.\frac{\partial\theta}{\partial z}\right|_{z=H} = 0 \tag{9}$$

Solving the problem in Laplace space gives Eq. (10).

$$\overline{\theta} = \sum_{k=0}^{N_k} \frac{P_{i,k}}{s^{(k/2)+1}} \frac{\cosh(\sqrt{s/a}(H-z))}{\cosh(\sqrt{s/a}(H-z_1))} \tag{10}$$

Unfortunately, expanding the hyperbolic functions in Eq. (10) and returning to the time domain in the manner suggested previously by Monde and co-workers [5,7,8] does not necessarily lead to a result that will converge for large values of $H$. Therefore we follow a slightly different procedure. Using the approach suggested in Carslaw and Jaeger [11] for heat conduction problems with small values of time, Eq. (10) can be rewritten as Eq. (11). Here we have made use of a Maclaurin series expansion of $1/(1-(-\exp[-2(s/a)^{1/2}(H-z_1)]))$.

$$\begin{aligned}\overline{\theta} = &\sum_{k=0}^{N_k} \frac{P_{i,k}}{s^{(k/2)+1}} e^{-\sqrt{s/a}(z-z_1)} \\ &+ \sum_{n=1}^{\infty}\sum_{k=0}^{N_k} (-1)^n \frac{P_{i,k}}{s^{(k/2)+1}} e^{-\sqrt{s/a}(2n(H-z_1)+z-z_1)} \\ &+ \sum_{n=0}^{\infty}\sum_{k=0}^{N_k} (-1)^n \frac{P_{i,k}}{s^{(k/2)+1}} e^{-\sqrt{s/a}(2n(H-z_1)+2H-z-z_1)}\end{aligned} \tag{11}$$

We can see that the first summation on the right of Eq. (11) is identical to the semi-infinite case, Eq. (3). The other two summations all involve terms containing expressions of the form:

$$\frac{e^{-\sqrt{s/a}B}}{s^{(k/2)+1}}$$

where $B$ is a positive number provided $2H$ is larger than $z+z_1$. For cases where $B$ is positive, the exact inverse Laplace transform [11] is given by:

$$L^{-1}\left\{e^{-\sqrt{s/a}B}/s^{k/2+1}\right\} = (4t)^{k/2}i^k\mathrm{erfc}(B/2\sqrt{at}) \tag{12}$$

The repeated integral of the complementary error function $i^k\mathrm{erfc}(\ )$ is defined and presented in a convenient form for implementation in Appendix II of Ref. [11]. Therefore, the basic function for estimating the surface temperature for a finite, but thick, one-dimensional solid that is insulated at $z=H$, is the semi-infinite result plus a correction involving summations of the error function as given by Eq. (13).

$$\begin{aligned}\theta = &\sum_{k=-1}^{N_k}\frac{G_{i,k}(t-t_i)^{k/2}}{\Gamma((k/2)+1)} + \sum_{n=1}^{\infty}\sum_{k=0}^{N_k}(-1)^n P_{i,k}(4(t-t_i))^{k/2}\\ &\times i^k\mathrm{erfc}\left(\frac{2n(H-z_1)-z_1}{2\sqrt{a(t-t_i)}}\right) + \sum_{n=0}^{\infty}\sum_{k=0}^{N_k}(-1)^n P_{i,k}(4(t-t_i))^{k/2}\\ &\times i^k\mathrm{erfc}\left(\frac{2n(H-z_1)+2H-z_1}{2\sqrt{a(t-t_i)}}\right)\end{aligned} \tag{13}$$

It should be mentioned that for large values of $B$, Eq. (12) rapidly approaches zero and Eq. (13) converges well. Therefore if $H$ is much larger than $z_1$, only a few terms are required in the summations to infinity. Eq. (13) can be used to replace Eq. (4) in the algorithm shown in Fig. 2.

## 6. Extension to two-dimensional problems

The two-dimensional problem has some additional complications, which require discussion. Consider for example the case of a thick two-dimensional plate of length, $L$, in Cartesian coordinates with a single line of sensors at depth $z_1$. The plate is insulated at both ends and at $z=H$. Like the one-dimensional finite plate, the approach used in [5] has trouble for large values of $H$. Therefore we present a modified procedure with some similarities to Section 5 above.

Unsteady heat conduction is governed by Eq. (14a), and the initial and boundary conditions are specified in Eqs. (14b)–(14e).

$$\frac{1}{a}\frac{\partial\theta}{\partial t} = \frac{\partial^2\theta}{\partial z^2} + \frac{\partial^2\theta}{\partial x^2} \tag{14a}$$

$$\theta|_{t=t_i} = 0 \tag{14b}$$

$$\left.\frac{\partial\theta}{\partial x}\right|_{x=0} = \left.\frac{\partial\theta}{\partial x}\right|_{x=L} = 0 \tag{14c}$$

$$\left.\frac{\partial\theta}{\partial z}\right|_{z=H} = 0 \tag{14d}$$

$$\theta|_{z=z_1} = \sum_{j=0}^{N_j} F_{i,j}(t-t_i)\cos\left(m_j\frac{x}{L}\right) \tag{14e}$$

The eigenvalues in Eq. (14e) are set as $m_j=j\pi$ where $(j=0,1,2,\ldots)$ in order to be in keeping with the boundary conditions given by Eq. (14c). To simplify the notation, from this point forward we will replace $(t-t_i)$ with $t$ and drop the subscript $i$. The approximating function, $F_j(\ )$ captures the variation with time of the coefficient of the $j$th eigenfunction based on measurements at depth $z_1$. In a similar manner to Eq. (2d) use is made of a polynomial series in the half power of time, but with an additional factor as shown in Eq. (15).

$$F_j(t) = e^{-am_j^2t/L^2}\sum_{k=0}^{N_k}\frac{P_{j,k}}{\Gamma((k/2)+1)}t^{k/2} \tag{15}$$

For the case of $m_j=0$ Eq. (15) is identical in form to Eq. (2d). Inclusion of the exponential factor in Eq. (15) makes the inverse Laplace transform much simpler and is a significant modification to the procedure previously proposed by Monde et al. [5,7,8]. Transforming Eq. (15) into Laplace space gives Eq. (16).

$$\overline{F}_j(s) = \sum_{k=0}^{N_k}\frac{1}{(s+(am_j^2/L^2))^{(k/2)+1}} \tag{16}$$

Solving the problem defined by Eq. (14) in the Laplace domain results in Eq. (17).

$$\begin{aligned}\overline{\theta}(z,x) = &\sum_{j=0}^{N_j}\overline{F}_j(s)\\ &\times\cos\left(\frac{m_jx}{L}\right)\frac{\cosh\left(\sqrt{(s/a)+(m_j^2/L^2)}(H-z)\right)}{\cosh\left(\sqrt{(s/a)+(m_j^2/L^2)}(H-z_1)\right)}\end{aligned} \tag{17}$$

Letting $p_j = s+(am_j^2/L^2)$ and combining Eqs. (16) and (17) we obtain Eq. (18), which has a similar form to the one-dimensional case expressed in Eq. (10).

$$\overline{\theta}(z,x) = \sum_{j=0}^{N_j}\cos(m_jx/L)\sum_{k=0}^{N_k}\frac{P_{j,k}}{p_j^{(k/2)+1}}\frac{\cosh\left(\sqrt{p_j/a}(H-z)\right)}{\cosh\left(\sqrt{p_j/a}(H-z_1)\right)} \tag{18}$$

We now proceed in exactly the same manner as for the one-dimensional case and then make use of the following shifting property of Laplace transforms:

$$L\{e^{\alpha t}f(t)\} = \overline{f}(s-\alpha)$$

The result for surface temperature in the time domain, as given by Eq. (19) has many similarities with Eq. (13) except for the summation over all eigenfunctions and the exponential factor arising from the shift.

$$\theta = \sum_{j=0}^{N_j} \cos(m_j x/L) \mathrm{e}^{-am_j^2 t/L^2} \theta_{1D}(t) \tag{19a}$$

$$\theta_{1D}(t) = \sum_{k=-1}^{N_k} \frac{G_{j,k} t^{k/2}}{\Gamma((k/2)+1)} + \sum_{n=1}^{\infty} \sum_{k=0}^{N_k} (-1)^n P_{j,k} (4t)^{k/2} \times \mathrm{i}^k \mathrm{erfc}\left(\frac{2n(H-z_1)-z_1}{2\sqrt{at}}\right) + \sum_{n=0}^{\infty} \sum_{k=0}^{N_k} (-1)^n P_{j,k} (4t)^{k/2} \times \mathrm{i}^k \mathrm{erfc}\left(\frac{2n(H-z_1)+2H-z_1}{2\sqrt{at}}\right) \tag{19b}$$

While the exponential factor in Eq. (15) makes the algebra relating to the Laplace transform very convenient, it places a strong restriction on the maximum size for the data window for eigenfunctions other than where $m_j = 0$. Because the exponential factor decays very quickly with time, even a simple function approximated by Eq. (15) will require huge numerical values for the coefficients $P_{j,k}$ if $t$ is large. It is some consolation that in the final solution given by Eq. (19), the same exponential factor, $\exp(-am_j^2 t/L^2)$, strongly damps and therefore reverses the effect of the large coefficients. However, numerically we have the unfavorable situation of very large numbers multiplied by very small numbers.

Fortunately, all the above problems can be overcome if we note that the eigenfunctions with large eigenvalues do not create temperature waves that penetrate deeply into the solid. Therefore at least some long-term history may be neglected for all cases except $m_j = 0$, which has exactly the same form as the one-dimensional case. In fact, by considering an analytical solution to the forward heat conduction problem on a semi-infinite solid (see Appendix 1) it can be shown that the effect of the long term thermal history for the $j$th eigenfunction decays in approximate proportion to $\mathrm{erfc}((am_j^2 t/L^2)^{1/2})$. This indicates that for 0.1% accuracy in relation to the contribution of the $j$th eigenfunction we do not need to consider any history before $am_j^2(t-t_0)/L^2 \approx 5.8$. Therefore, instead of using $t_0 = 0$ as in Figs. 1(a) and 2, we use Eq. (20) where $t_0$ is the starting point for the very first data window for the $j$th eigenfunction.

$$t_0 = t - C_3 L^2/(am_j^2) \tag{20}$$

The limit of $C_3 = 5.8$ still may cause the appearance of fairly large values for the coefficients $P_{j,k}$, but the numerical problems mentioned above are avoided. Also, a smaller starting window means fewer calculation windows are required and the computation time is reduced.

The final algorithm for the two-dimensional case is similar to Fig. 2 except that each eigenfunction component is considered separately and the first window size is set smaller as $m_j$ becomes larger. Another small difference for the present two-dimensional formulation is that we have found that the results are significantly smoother if the half-polynomial function is restricted to five terms ($N_k = 4$). This is a little lower than the optimum ($5 < N_k < 8$) recommended by Monde et al. [7] and probably is due to the different approach in the formulation. Also, the interpolation procedure given in [5] is followed and the coefficients of the higher order eigenfunctions are damped using Eq. (21) before applying the inverse solution. In Eq. (21) $m_{j\mathrm{cut}}$ is the 'cut-off' eigenvalue for the Butterworth type smoother corresponding to the number of sensors plus 3 [5].

$$F_j|_{\mathrm{smooth}} = F_j|_{\mathrm{raw}}/(1 + (m_j/m_{j\mathrm{cut}})^4) \tag{21}$$

Before concluding this section it is worth noting that for large values of $m_j$, even the first window as defined by Eq. (20) may be so small that it contains only one data point. In such cases, rather than ignore the contribution of that particular eigenfunction completely we have found it is better to first fit a half-polynomial function to the coefficients for a larger window of the data and then interpolate several points near the time of interest. Eq. (15) can then be fitted to the interpolated points.

## 7. Application to problems with large Fourier numbers

From the theme of the paper the reader may have the impression that the present method cannot be applied to data where the Fourier number based on the total time is large, or if the solid is thermally thin for the largest timescale of interest. Actually, this is not the case. To consider problems where the Fourier number based on the second boundary at $z_2$ is large all we need to do is shift the position of $t_0$ so that the largest Fourier number used in the calculation is restricted to a value that can be handled without loss of accuracy. From a computational perspective it is desirable to limit the maximum size since the largest Fourier number influences the number of terms required in the summations to infinity in Eqs. (13) and (19b). In the previous section and in Appendix 1 we demonstrated that the long-term history of high frequency eigenfunctions could be neglected for a semi-infinite solid. If the solid is finite then the long-term history even for the case where $m_j = 0$ can be neglected based on the Fourier number for the position of the second boundary. A Fourier number of $a(t-t_0)/z_2^2 = 3.2$ (for 0.0001% accuracy) can be used as a suitable criterion where the heat flux boundary is zero at $z = z_2$. Note that this value is double that required for the same accuracy when the temperature is measured at $z_2$ [5] to allow time for thermal waves to be reflected back from the insulated boundary. This criterion translates to using Eq. (22) (with $C_4 = 3.2$) instead of $t_0 = 0$ in Fig. 2 for the finite one-dimensional case.

$$t_0 = \mathrm{Max}(0,\ t - C_4 L^2/a) \tag{22}$$

For the two-dimensional case, Eq. (22) should be used for the component where $m_j = 0$. Therefore, in principle if the sensor is infinitesimally small, the present procedure can be applied to resolve any time scales that are much greater than the minimum detectable time period as approximated by $at_{\min}/z_1^2 \approx 0.1$.

## 8. Application to problems with different boundary conditions

The above formulations are suitable for problems where the domain can be treated as a semi-infinite solid or if at $z = z_2$ the boundary is perfectly insulated. Strictly speaking, neither of these boundaries exists in reality. However, as mentioned, if the Fourier number based on the total time and the total thickness of the solid is less than about 0.1 then the solid may be considered semi-infinite for many practical purposes. Also if the actual heat loss through the insulation is small compared with the heat flux at the surface of interest then the above finite formulation can be used. Nonetheless, if we can estimate the heat loss at $z = z_2$, then it may be desirable to modify the boundary condition in the formulation to better account for a known heat flux. Likewise, if we have a thick solid with a few sensors at $z = z_2$ we may wish to use a temperature boundary condition to close the problem rather than heat flux. In fact, the present approach can be modified easily for such cases. The formulation of the solution for these two important cases is given in Appendix 2.

It should be mentioned that the approach in [5] is preferred for the case of sensors at two depths if both depths are reasonably close to the surface. This is because the procedure is faster and simpler (compare Fig. 1(b) and (a)) and there is less room for accumulation of numerical errors. The present method has the merit that the position of $z_2$ can be far from the surface and thus fewer sensors are required at this boundary.

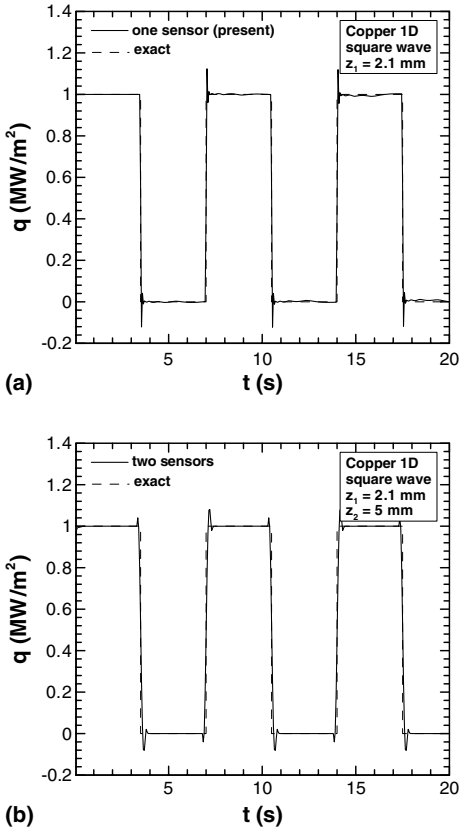


Fig. 4. Inverse solutions for surface heat flux on a semi-infinite solid where the exact solution is a square wave in time (a) one sensor using present approach and (b) two sensors with moving window.

## 9. Results

### 9.1. One-dimensional semi-infinite case

Fig. 4 shows the predicted surface heat flux for a case where for the exact result, the heat flux on the boundary is in the form of a square-wave with respect to time. The sensor response for Fig. 4 is given in Fig. 1 assuming the convention (used in quenching experiments) that heat loss from the solid is positive. Fig. 4(a) shows the present result for one sensor and Fig. 4(b) shows the case for two sensors. The agreement between the two cases and with the exact result is quite good. The overshoots near the step changes is a result of the imperfect data fit near the sudden change in temperature inside the solid and the general inability of the inverse solution to fully resolve high frequency components.

Although not a major issue, it may be observed in Fig. 4(b) that the solution overshoots both before and after each step change in heat flux while in Fig. 4(a) the overshoot only occurs after the step change. This difference is not so much due to the different method but simply a result of how much future data is included in the calculation. Fig. 4(b) follows the recommendations of [5] to specify the size of $(t_f - t)$ which give a larger value than Eq. (8) in the present study. If the same amount of future data is used in both methods then the overshoot before the step change becomes similar.

Considering the excellent performance of the two-sensor approach with only a small amount of data as shown in Fig. 4(b) (cf. Fig. 1(b)), one may wonder if it also is possible to obtain good results with a small window of data and only one sensor. Unfortunately this is not the case. Fig. 5(a) shows the surface heat flux for the same case as in Fig. 4 but calculated based on temperature data from a single moving window and only one sensor. The size of the window was the same as that used for Fig. 4(b). The poor agreement between the calculation and exact result in Fig. 5(a) verifies that for a single sensor and a far-field boundary condition, the long-term history should not be neglected completely.

From another angle, to confirm the value of the correction terms in Eq. (1d), Fig. 5(b) gives the inverse solution where only the first term on the right of Eq. (1d) is included. For the first 3 s in Fig. 5(b) the predictions are excellent. This is a reflection of how well the polynomial in the half-power of time can approximate the data before any sudden changes occur. Once the data begins oscillating however, the polynomial without correction can no longer follow the data accurately.

### 9.2. One-dimensional finite case

A further case that deserves attention is a finite slab with one surface $(z = 0)$ experiencing the same boundary

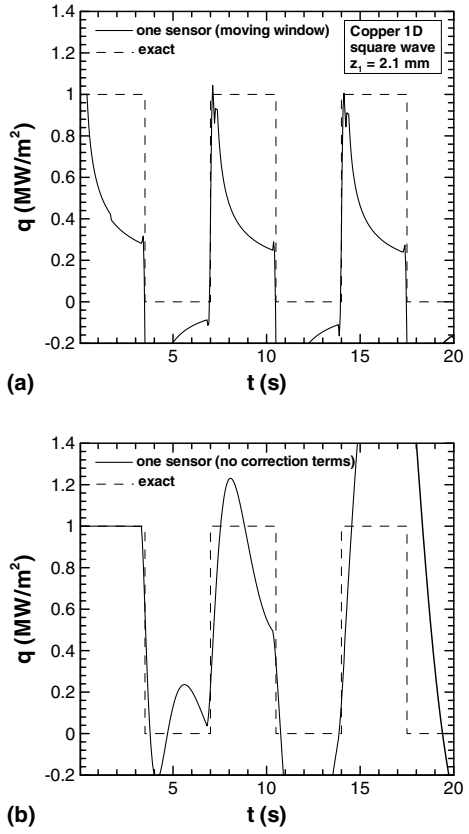


Fig. 5. Surface heat flux for IHCP where exact answer is a square wave (a) moving window with one sensor and no long-term history and (b) Eq. (1d) with no correction terms.

condition as in Fig. 4 and the other surface ($z = H$) being insulated. For this case the surface heat flux counterpart to Eq. (13) is applicable. Fig. 6 gives the inverse solution results for surface heat flux. The agreement between the exact and the present thick-plate solution is excellent.

For reference, the semi-infinite solid solution is also applied to the same problem in Fig. 6. Until about 7 s, the semi-infinite result agrees well with the finite solution. After about 8 s in Fig. 6 the semi-infinite result begins to drift noticeably from the correct solution. This is expected since the time for the thermal wave to penetrate 59 mm into a copper plate is of the order of 3–4 s and the effects will not be felt by the sensor near the surface for an additional few seconds to allow for the time for the wave to be 'reflected' back from the insulated boundary.

### 9.3. Two-dimensional finite case

For verification of the two-dimensional formulation we have selected data from impinging jet quenching experiments by Hammad et al. [9]. Their experiment was performed on a cylindrical brass block 94 mm diameter and 59 mm height. In comparison with heat extracted by the water jet from the test surface, heat losses by radiation and natural convection in air from the top may be considered small in this case. This provides justification for an

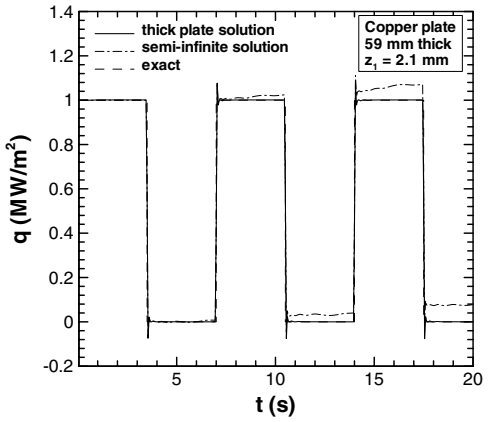


Fig. 6. Present predictions of surface heat flux for copper plate insulated at $z = 59$ mm.

insulated boundary at $z = 59$ mm. In any case up until time of about 11 s the test piece should behave much like a semi-infinite solid. Hammad et al. measured temperatures at 16

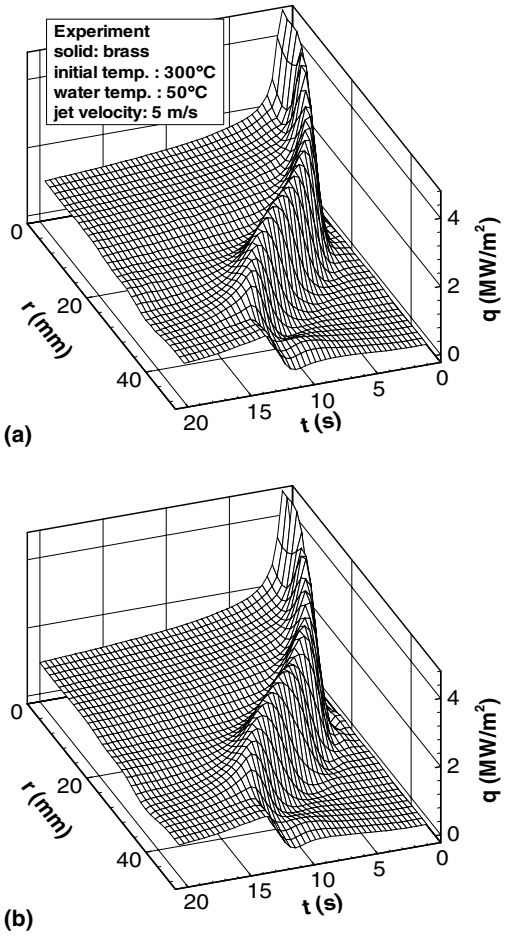


Fig. 7. Surface heat flux calculated from experimental data of Hammad et al. [9]. (a) Present solution using only data from sensors at depth $z_1 = 2.1$ mm and assuming insulated boundary condition at $z = 59$ mm. (b) Using data from sensors at $z_1 = 2.1$ mm and $z_2 = 5.0$ mm (Fig. 7(b) adapted from [5]).

locations in the solid. Eight sensors were at a depth of 2.1 mm from the surface and the remaining eight were 5.0 mm below the surface. Unlike Eq. (19a) this example requires cylindrical coordinates. However, as pointed out in [5], the formulation for cylindrical coordinates only requires that $\cos(m_j x/L)$ in Eq. (19a) be replaced by the Bessel function, $J_0(m_j r/R)$, where $R$ is the radius of the cylinder, $r$ is the radial position and $m_j$ is now the $j$th positive root of $J_1(m_j) = 0$ for perfect insulation at $r = R$.

Using only the first depth and the zero heat flux boundary at $z = 59$ mm, the present inverse solution gives the heat flux distribution shown in Fig. 7(a). Fig. 7(b) shows previous results [5] based on both depths. Fig. 8 gives the difference between the two cases in Fig. 7. The maximum difference of about 0.4 MW/m$^2$ appears in the region where the heat flux is changing rapidly. The peak heat flux in both cases is similar being a little over 4 MW/m$^2$. In general, the agreement between the two cases in Fig. 7 is quite acceptable. Differences partly may be due to uncertainties in the sensor readings, changes in thermal properties with temperature and heat losses through the top and sides of the test piece. Also, because the final window in the present approach tends to be smaller than the moving window for the previous approach [5] we may expect less smoothing of the higher frequency components for Fig. 7(a). For this reason Fig. 7(a) has a slightly rougher appearance than Fig. 7(b) and in fact this may be an important cause for the differences in the calculated surface distributions.

Fig. 9 shows the calculated surface temperature distributions for the same case as in Fig. 7. The agreement between the present calculations using Eq. (19) and the results using the two-depth approach is excellent. The maximum temperature difference between the two cases occurs in the region where the temperature changes rapidly and is about 10°C, which is less than 5% of the total temperature drop during the quench. This agreement again demonstrates the usefulness of the present approach.

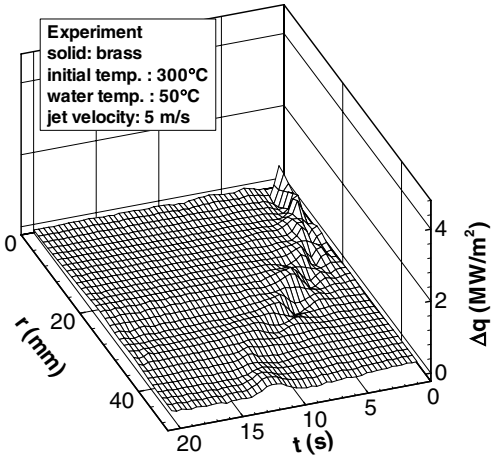


Fig. 8. Difference in surface heat flux predictions between the two methods shown in Fig. 7.

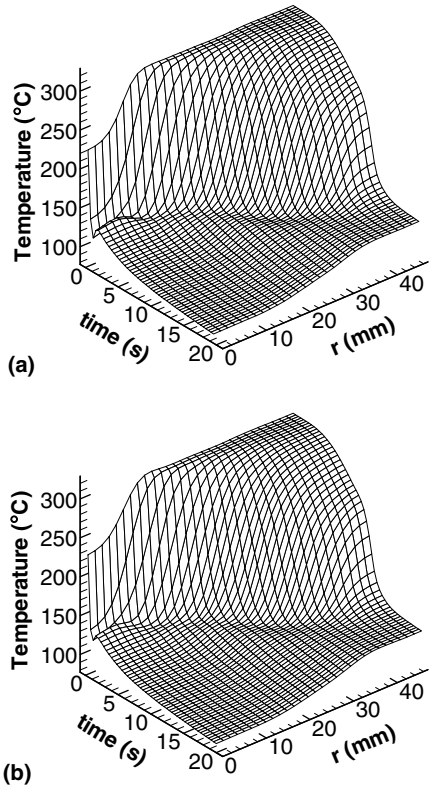


Fig. 9. Surface temperature calculated from experimental data of Hammad et al. [9]. (a) Present solution using only data from sensors at depth $z_1 = 2.1$ mm and assuming insulated boundary condition at $z = 59$ mm. (b) Using data from sensors at $z_1 = 2.1$ mm and $z_2 = 5.0$ mm.

## 10. Conclusions

Based on the above results and discussion the following conclusions can be drawn.

1. The present inverse solutions are suitable for both one- and two-dimensional heat conduction problems in simple geometry with sensors at one depth from the surface and a far-field boundary.
2. By changing the boundary condition in the formulation, the present method also can be applied to cases with sensors at two depths where the second depth is far from the surface.
3. The present method can be applied to thermally thin solids but due to the additional complications in the procedure, other approaches as in [5] may be preferred for such cases.
4. The proposed form (Eq. (1d)) for approximating the measured data performs well.
5. Long-term history of the low frequency components in the data cannot be neglected if a far-field boundary is used in the inverse solution.
6. Long-term history of the high frequency components in both time and space can be neglected.
7. High frequency components in the short-term history are important and must not be neglected.

Finally, the authors are pleased to make available openly the software developed to implement the present inverse solutions. Interested readers should contact the Monde laboratory.

**Acknowledgement**

Support from the 'Grant-in-Aid for Scientific Research (C), 2005' is acknowledged gratefully.

## Appendix 1. Justification for neglecting long-term history of higher frequency eigenfunctions

Due to the numerical problems associated with using a large data window mentioned in Section 6, the success or failure of the present two-dimensional formulation hinges on whether or not long-term history can be neglected for the eigenfunction components where $m_j$ is large.

By way of illustration, consider the following forward heat conduction problem.

$$\frac{1}{a}\frac{\partial T}{\partial t} = \frac{\partial^2 T}{\partial z^2} + \frac{\partial^2 T}{\partial x^2} \tag{A1}$$

$$T|_{t=0} = 0 \tag{A2}$$

$$\left.\frac{\partial T}{\partial x}\right|_{x=0} = \left.\frac{\partial T}{\partial x}\right|_{x=L} = 0 \tag{A3}$$

$$T|_{z\to\infty} = 0 \tag{A4}$$

$$T|_{z=0} = A\cos(m_j x/L)\ \ (t < t_1) \tag{A5a}$$

$$T|_{z=0} = 0\ \ (t \geqslant t_1) \tag{A5b}$$

Eqs. (A1)–(A4), (A5a), (A5b) represent a two-dimensional problem where up until time $= t_1$ the temperature boundary condition at $z = 0$ is given by the cosine function expressed in Eq. (A5a). After time $t_1$, the surface temperature is zero (i.e., homogeneous) and we wish to examine how long it takes for the temperature distribution in the solid to return to zero. In other words, how long does it take for the semi-infinite solid to 'forget' the boundary condition (A5a) for the eigenfunction corresponding to the eigenvalue, $m_j$?

Using Laplace transforms, the exact solution to Eqs. (A1)–(A5) can be derived as given in Eq. (A6).

$$T = A\cos(m_j x/L)\phi(z,t) \tag{A6a}$$

$$\begin{aligned}\phi(z,t) = {} & \frac{e^{-m_j z/L}}{2}\operatorname{erfc}\left[\frac{z}{2\sqrt{at}} - \sqrt{\frac{am_j^2 t}{L^2}}\right] \\ & + \frac{e^{m_j z/L}}{2}\operatorname{erfc}\left[\frac{z}{2\sqrt{at}} + \sqrt{\frac{am_j^2 t}{L^2}}\right] \\ & - \frac{e^{-m_j z/L}}{2}\operatorname{erfc}\left[\frac{z}{2\sqrt{a(t-t_1)}} - \sqrt{\frac{am_j^2 (t-t_1)}{L^2}}\right] \\ & - \frac{e^{m_j z/L}}{2}\operatorname{erfc}\left[\frac{z}{2\sqrt{a(t-t_1)}} + \sqrt{\frac{am_j^2 (t-t_1)}{L^2}}\right]\end{aligned} \tag{A6b}$$

Now to understand clearly the transient behavior of Eq. (A6) after $t_1$, we consider only the case where $t_1$ is large. The first two terms on the right in Eq. (A6b) then approach the steady-state result, $\exp(-m_j z/L)$. Eq. (A6b) then becomes Eq. (A7).

$$\phi(z,t) \approx e^{-\zeta} - \frac{e^{-\zeta}}{2}\operatorname{erfc}\left[\frac{\zeta}{2\sqrt{\tau}} - \sqrt{\tau}\right] - \frac{e^{\zeta}}{2}\operatorname{erfc}\left[\frac{\zeta}{2\sqrt{\tau}} + \sqrt{\tau}\right] \tag{A7a}$$

$$\zeta = m_j z/L \tag{A7b}$$

$$\tau = am_j^2 (t - t_1)/L^2 \tag{A7c}$$

Although not immediately obvious it can be verified numerically that for positive $(t - t_1)$ and $z$, $\phi$ is always in the range from zero to one and as time becomes larger for any value of $z$, Eq. (A7a) approaches zero at a slightly faster rate than $\operatorname{erfc}(\tau^{1/2})$. Thus for this particular case, the long-term history, or the effect of the boundary condition before time $= t_1$, safely may be considered to vanish in proportion to $\operatorname{erfc}((am_j^2(t-t_1)/L^2)^{1/2})$.

While the above illustration cannot be considered a rigorous proof, it demonstrates the general principle that for conduction in solids, the long-term history of high frequency spatial components is quickly forgotten. Naturally, the same principle will apply for both forward and inverse problems. Also in the above, the dimensionless group given by Eq. (A7c) is shown to be the key for determining an appropriate time-scale before which data may be neglected.

## Appendix 2. Formulation for other boundary conditions

The present approach may be modified easily for boundary conditions at $z_2$ other than zero heat flux or the semi-infinite condition. The purpose of this appendix is to present some additional important cases. For brevity, we give only the result and leave the derivation as an exercise for the reader. In all of the following, the solutions are given for any value of $z$ from 0 to $z_2$. This makes it easier to extract the surface heat flux by differentiation or calculate the temperature distribution in the solid if desired. Note [11] that the first derivative of the repeated integral of the complementary error function, $i^k\operatorname{erfc}(x)$ is $-i^{k-1}\operatorname{erfc}(x)$. Substitute $z = 0$ to obtain the result at the surface.

*A2.1. 1D finite slab, constant heat flux, $q_0$, out of slab at $z = z_2$, temperature at $z = z_1$ a function of time given by Eq. (1d)*

$$T(z,t) - T_0 = \frac{2q_0\sqrt{at}}{\lambda}\sum_{n=0}^{\infty}((-1)^n g_n(z,t)) + \sum_{i=0}^{N_{\text{corr}}}\theta_i(z,t) \tag{A8a}$$

$$\begin{aligned}g_n(z,t) = {} & \operatorname{ierfc}\left(\frac{2n(z_2 - z_1) + z_2 - 2z_1 + z}{2\sqrt{at}}\right) \\ & - \operatorname{ierfc}\left(\frac{2n(z_2 - z_1) + z_2 - z}{2\sqrt{at}}\right)\end{aligned} \tag{A8b}$$

$$\theta_i(z,t) = \sum_{n=0}^{\infty}(-1)^n h((2n(z_2-z_1)+z-z_1),t) + \sum_{n=0}^{\infty}(-1)^n h((2n(z_2-z_1)+2z_2-z-z_1),t) \quad \text{(A9)}$$

where the function $h(B,t)$ is specified by Eq. (A10).

$$h(B,t) = \sum_{k=0}^{N_k} P_{i,k}(4(t-t_i))^{k/2}\mathrm{i}^k\mathrm{erfc}\left(\frac{B}{2\sqrt{a(t-t_i)}}\right) \quad (B \geqslant 0) \quad \text{(A10a)}$$

$$h(B,t) = \sum_{k=-1}^{N_k} \frac{G_{i,k}(t-t_i)^{k/2}}{\Gamma((k/2)+1)} \quad (B<0) \quad \text{(A10b)}$$

The coefficients, $G_{i,k}$ in Eq. (A10b) are determined by equating coefficients in Eq. (A10c).

$$\sum_{k=-\infty}^{N_k}\frac{G_{i,k}}{s^{(k/2)+1}} = \sum_{n=0}^{N_k}\frac{P_{i,n}}{s^{(n/2)+1}}\sum_{j=0}^{\infty}\frac{1}{j!}\left(\frac{-B}{\sqrt{a}}\right)^j s^{j/2} \quad \text{(A10c)}$$

In Eq. (A8b) it was assumed that $z_2 \geqslant 2z_1$ but this restriction does not apply to Eq. (A8a) if $q_0$ is zero.

*A2.2. 1D finite slab, temperature at $z = z_1$ a function of time given by Eq. (A11a), temperature at $z = z_2$ a function of time given by Eq. (A11b)*

$$(T-T_0)|_{z=z_1} = \sum_{i=0}^{N_{\mathrm{corr}}}\sum_{k=0}^{N_k} P_{i,k}^{(1)}\frac{(t-t_i)^{k/2}}{\Gamma((k/2)+1)} \quad \text{(A11a)}$$

$$(T-T_0)|_{z=z_2} = \sum_{i=0}^{N_{\mathrm{corr}}}\sum_{k=0}^{N_k} P_{i,k}^{(2)}\frac{(t-t_i)^{k/2}}{\Gamma((k/2)+1)} \quad \text{(A11b)}$$

Eqs. (A12) and (A13) give the solution.

$$T(z,t) - T_0 = \sum_{i=0}^{N_{\mathrm{corr}}}\theta_i(z,t) \quad \text{(A12)}$$

$$\theta_i(z,t) = \sum_{n=0}^{\infty}h^{(1)}((2n(z_2-z_1)+z-z_1),t) - \sum_{n=0}^{\infty}h^{(1)}((2n(z_2-z_1)+2z_2-z-z_1),t) + \sum_{n=0}^{\infty}h^{(2)}((2n(z_2-z_1)+z_2-z),t) - \sum_{n=0}^{\infty}h^{(2)}((2n(z_2-z_1)+z_2+z-2z_1),t) \quad \text{(A13)}$$

Again the function $h(B,t)$ in Eq. (A13) is given by Eq. (A10) but noting that the superscript is included so that $h^{(1)}(B,t)$ and $h^{(2)}(B,t)$ indicates to use the coefficients $P_{i,k}^{(1)}$ and $P_{i,k}^{(2)}$, respectively. Eqs. (A12) and (A13) are preferred to the method in [5] if $z_2$ is not close to the surface.

*A2.3. 2D finite slab, temperature at $z = z_1$ a function of time and x position given by Eq. (A14a), temperature at $z = z_2$ a function of time and x given by Eq. (A14b)*

$$T|_{z=z_1} - T_0 = \sum_{j=0}^{N_j}\cos\left(m_j\frac{x}{L}\right)\sum_{i=0}^{N_{\mathrm{corr},j}} \times\left[\mathrm{e}^{-am_j^2(t-t_i)/L^2}\sum_{k=0}^{N_k}P_{i,k,j}^{(1)}(t-t_i)^{k/2}/\Gamma((k/2)+1)\right] \quad \text{(A14a)}$$

$$T|_{z=z_2} - T_0 = \sum_{j=0}^{N_j}\cos\left(m_j\frac{x}{L}\right)\sum_{i=0}^{N_{\mathrm{corr},j}} \times\left[\mathrm{e}^{-am_j^2(t-t_i)/L^2}\sum_{k=0}^{N_k}P_{i,k,j}^{(2)}(t-t_i)^{k/2}/\Gamma((k/2)+1)\right] \quad \text{(A14b)}$$

The solution is given by Eq. (A15).

$$T(x,z,t) - T_0 = \sum_{j=0}^{N_j}\cos\left(m_j\frac{x}{L}\right)\sum_{i=0}^{N_{\mathrm{corr},j}}\mathrm{e}^{-am_j^2(t-t_i)/L^2}\theta_{i,j}(z,t) \quad \text{(A15)}$$

Notice in Eq. (A15) that the number of corrections, $N_{\mathrm{corr},j}$ may be different depending on the eigenfunction (cf. Section 6 above).

$$\theta_{i,j}(z,t) = \sum_{n=0}^{\infty}h_j^{(1)}((2n(z_2-z_1)+z-z_1),t) - \sum_{n=0}^{\infty}h_j^{(1)}((2n(z_2-z_1)+2z_2-z-z_1),t) + \sum_{n=0}^{\infty}h_j^{(2)}((2n(z_2-z_1)+z_2-z),t) - \sum_{n=0}^{\infty}h_j^{(2)}((2n(z_2-z_1)+z_2+z-2z_1),t) \quad \text{(A16)}$$

Although the form of the function $h_j^{(1)}(B,t)$ in Eq. (A16) is the same as in Eq. (A10), to show clearly that the coefficients are different depending on the eigenfunctions, $h_j^{(1)}(B,t)$ is repeated in full for depth (1) in Eq. (A17).

$$h_j^{(1)}(B,t) = \sum_{k=0}^{N_k}P_{i,k,j}^{(1)}(4(t-t_i))^{k/2}\mathrm{i}^k\mathrm{erfc}\left(\frac{B}{2\sqrt{a(t-t_i)}}\right) \quad (B\geqslant 0) \quad \text{(A17a)}$$

$$h_j^{(1)}(B,t) = \sum_{k=-1}^{N_k}\frac{G_{i,k,j}^{(1)}(t-t_i)^{k/2}}{\Gamma((k/2)+1)} \quad (B<0) \quad \text{(A17b)}$$

The coefficients, $G_{i,k,j}$ in Eq. (A17b) are determined by equating coefficients in Eq. (A17c).

$$\sum_{k=-\infty}^{N_k}\frac{G_{i,k,j}^{(1)}}{s^{(k/2)+1}} = \sum_{n=0}^{N_k}\frac{P_{i,n,j}^{(1)}}{s^{(n/2)+1}}\sum_{p=0}^{\infty}\frac{1}{p!}\left(\frac{-B}{\sqrt{a}}\right)^p s^{p/2} \quad \text{(A17c)}$$

## References

[1] O.R. Burggraf, An exact solution of the inverse problem in heat conduction theory and applications, ASME J. Heat Transfer 86 (1964) 373–382.
[2] E.M. Sparrow, A. Haji-Sheikh, T.S. Lundgren, The inverse problem in transient heat conduction, ASME J. Appl. Mech. 31 (1964) 369–375.
[3] M. Imber, Temperature extrapolation mechanism for two-dimensional heat flow, AIAA J. 12 (8) (1974) 1089–1093.
[4] M. Shoji, Study of inverse problem of heat conduction, Trans. JSME 44 (381) (1978) 1633–1643 (in Japanese).
[5] P.L. Woodfield, M. Monde, Y. Mitsutake, Implementation of an analytical inverse heat conduction technique to practical problems, Int. J. Heat Mass Transfer 49 (2006) 187–197.
[6] M. Monde, Y. Mitsutake, A new estimation method of thermal diffusivity using analytical inverse solution for one-dimensional heat conduction, Int. J. Heat Mass Transfer 44 (2001) 3169–3177.
[7] M. Monde, H. Arima, Y. Mitsutake, Estimation of surface temperature and heat flux using inverse solution for one-dimensional heat conduction, J. Heat Transfer 125 (2003) 213–223.
[8] M. Monde, H. Arima, W. Liu, Y. Mitsutake, J.A. Hammad, An analytical solution for two-dimensional inverse heat conduction problems using Laplace transform, Int. J. Heat Mass Transfer 46 (2003) 2135–2148.
[9] J. Hammad, Y. Mitsutake, M. Monde, Movement of maximum heat flux and wetting front during quenching of hot cylindrical block, Int. J. Therm. Sci. 43 (2004) 743–752.
[10] A.K. Mozumder, M. Monde, P.L. Woodfield, Delay of wetting propagation during jet impingement quenching for a high temperature surface, Int. J. Heat Mass Transfer 48 (2005) 5395–5407.
[11] H.S. Carslaw, J.C. Jaeger, Conduction of Heat in Solids, second ed., Oxford University Press, 2003.